Computer Optimization of Transducer Transfer Functions Using Constraints on Bandwidth, Ripple, and Loss

Theodore L. Rhyne, *Member, IEEE*

***Abstract*—Transducers, having one piezoelectric layer near its half-wave resonance and N quarter-wave layers, are designed using computer optimization to adjust the thicknesses and impedances of the various layers so as to fit the resulting transfer function to a target function. An augmented Mason model is used to evaluate the transducer. Optimization of fit is by a steepest descent algorithm. Essentially error-free fits are achieved for target functions that match the underlying dynamics. By applying classical filter theory to a lumped-element transducer model, the transducers dynamics are identified as all-pole filters, which are characterized by polynomials of order N to $N+1$. The design methodology is tested by designing a series of low-loss transducers that explore fractional bandwidths from 45 to 116%. From these studies there appears to be constraints on the minimum Q of the poles, and other properties. Typical power transfer efficiencies of -1 dB are achieved by impedance scale matching. Using a second-order Fano bound, it is shown that the matching layers function as an optimal compensation network for low-loss flat bandpass transducers. Finally, by the inclusion of loss, lower Q poles are demonstrated with a Bessel transducer.**

I. Introduction

THE fundamental model of a piezoelectric layer transducer is that of Mason [1], wherein a piezoelectric layer is poled through the thickness of the layer and electrical terminals are attached as thin conductive layers on both faces. The layer may be acoustically loaded on either or both of the two faces. There are several well-known models that are interpretations of the fundamental Mason model including: Redwood [2], KLM [3], and the lumped-element model [4].

An important class of transducer consists of a piezoelectric layer operating near its half-wave resonance, which is loaded on one face to a water-like acoustic media with interposed nearly quarter-wave matching layers and on the other face to a backing material. The matching layers act as a filter and provide an impedance transformation between the water-like media and the piezoelectric layer. These methods have been well studied in the realm of microwave and radio frequency engineering [5], [6].

Many methods for the design of transducer transfer functions have been advanced which specify the choice of impedances and thicknesses for the layers using analytical approximations. The most fundamental designs treat single and double matching layers together with a low-loss backing, as in the work of Kossoff [7]. The impedance choices presented by DeSilets *et al.* were a significant advance [8]. Inoue *et al.* and Goll *et al.*, among others, have approached the design of transducers with three and more matching layers [9]–[11].

The application of computer optimization to transducer design offers the opportunity to manage the complexity of designing resonant layers and construction layers (e.g., bonding, metallization, etc.). Selfridge *et al.* [12] and later Lockwood and Foster [13] optimized a "badness" function of the impulse response. Alternatively, Van Crombruge and Thompson used nonlinear goal programming to optimize the transfer function of a transducer [14]. These methods demonstrate the capability of algorithms to handle the complexity of realistic designs while satisfying optimizing criteria. However, the underlying resonances of the transducer impose constraints on the universe of possible transfer functions. An approach is sought that combines computer optimization with insights into the limitations imposed by the transducer resonances.

The objective of this paper is to determine a methodology for computer design of transducer transfer functions and their impulse responses. The transducer and its parameters are defined using a modified Mason model plus a model for the acoustic layers. The transducer optimization is defined using a "target" transfer function and an error function, which is minimized by standard methods. By applying classical filter theory to the lumped-element model, it is determined that the transducer transfer function has an all-pole characteristic. A computer design process is defined using all-pole target functions. The design methodology is used to explore a series of low-loss two-matching-layer designs and achieve virtually error-free optimization of the polynomial target functions. The underlying constraints on the characteristic poles for low-loss designs are explored by examining the series of progressively wider bandwidth designs using certain classic polynomial filters (Butterworth, Bessel, Chebyshev, etc.). It is noted that with proper impedance scaling and low loss, the power transfer function may be made extremely efficient over significant bandwidths. A second-order Fano performance bound, relating bandwidths and reflection coefficients, is applied to the matching layers as a compensating filter. It is found that the performance of series of transducers generally approaches the bound. In a rigorous test, a fifth-order lossless transducer demonstrates excellent agreement with the bound. This proves the optimality of the multilayer compensation for flat transfer functions. Finally, by including loss it is demonstrated that

Manuscript received June 23, 1995; revised May 14, 1996.

The author is with the Applied Science Laboratory, GE Medical Systems, Milwaukee, WI 53201 USA.

Publisher Item Identifier S 0885-3010(96)07864-1.

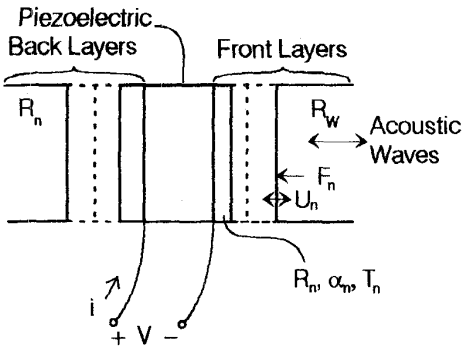

Fig. 1. Physical construction of the transducer having one piezoelectric layer that is electrically layered at its faces and multiple "front" and "back" layers ending in half spaces.

lower Q (all-pole) transfer functions may be achieved, with the example of a fourth-order Bessel.

II. Transfer Function Calculation

The class of transducer considered is shown in Fig. 1, with a piezoelectric layer acoustically coupled on its "front" and "back" faces to multiple acoustic layers ending in half spaces, and electrically coupled to a terminal pair formed by conductive layers on the piezoelectric layer. The transducer is electrically excited through the terminal pair, radiates waves from the front acoustic structure, receives acoustic waves at the front, and observes the waves in an electrical network connected to the electrical terminals.

The operation of the transducer is analyzed using equivalent electromechanical circuit models for the transducer and the electrical network. The fundamental model for a piezoelectric layer transducer is the modified Mason model given in

$$\begin{bmatrix} F_1 \\ F_2 \\ V \end{bmatrix} = \begin{bmatrix} AR_c \dfrac{Z^2+e^{-2\alpha}}{Z^2-e^{-2\alpha}} & 2AR_c \dfrac{Ze^{-\alpha}}{Z^2-e^{-2\alpha}} & \dfrac{h}{j\omega} \\ 2AR_c \dfrac{Ze^{-\alpha}}{Z^2-e^{-2\alpha}} & AR_c \dfrac{Z^2+e^{-2\alpha}}{Z^2-e^{-2\alpha}} & \dfrac{h}{j\omega} \\ \dfrac{h}{j\omega} & \dfrac{h}{j\omega} & \dfrac{l}{A\epsilon^S j\omega} + R_0 \end{bmatrix} \cdot \begin{bmatrix} U_1 \\ U_2 \\ I \end{bmatrix} \quad (1)$$

where

F_1, F_2	force on the faces (N);
U_1, U_2	velocity of faces (m/s);
Z	time shift operator $\exp(jT)$;
ω	radian frequency (rad/s);
T	transit time across the layer $= l/v^D$ (s);
R_c	specific acoustic impedance of the layer (Rayl);
A	area of the layer (m^2);
ϵ^S	dielectric constant at fixed strain (F/m);
l	thickness of the layer (m);
h	piezoelectric constant (N/C);
h	$h = k_T(v^D R_c/C_0 l)$ [15];
v^D	velocity at constant displacement (m/s);
C_0	capacitance at constant strain $= \epsilon^S A/l$ (F);
k_T	piezoelectric coupling constant (transversely clamped);
V, I	electrical voltage and current (V, A);
j	the unit imaginary number;
α	one-way loss (which may be a function of frequency) (Np);
R_0	dielectric loss resistance, which may be a function of frequency (Ω).

The piezoelectric layer possesses two mechanical ports and one electrical port. The front and back faces of the piezoelectric layer are fully described by the mechanical terminal variables of velocity and force, U and F, while the electrical terminals are fully described by the voltage and current, V and I. The upper left square in the matrix can be interpreted as a lossy acoustic transmission line, the lower right entry represents the series reactance of a capacitance plus a dielectric loss resistance, R_0. Piezoelectric coupling is expressed by the piezoelectric constant, h, in the cross terms. The form of (1) is modified from the Mason model of [4] with the addition of loss to the acoustic transmission line and dielectric loss to the static capacitance.

The Mason model may be readily interconnected with acoustic and electrical loads to complete the transducer model. The transducer is constrained to have multiple layers with the same outside dimensions, which load both faces of the piezoelectric layer, as shown in Fig. 1. The nth layer is characterized using the expression

$$\begin{bmatrix} F_{1,n} \\ F_{2,n} \end{bmatrix} = \begin{bmatrix} AR_n \dfrac{Z_n^2+e^{-2\alpha_n}}{Z_n^2-e^{-2\alpha_n}} & 2AR_n \dfrac{Z_n e^{-\alpha_n}}{Z_n^2-e^{-2\alpha_n}} \\ 2AR_n \dfrac{Z_n e^{-\alpha_n}}{Z_n^2-e^{-2\alpha_n}} & AR_n \dfrac{Z_n^2+e^{-2\alpha_n}}{Z_n^2-e^{-2\alpha_n}} \end{bmatrix} \cdot \begin{bmatrix} U_{1,n} \\ U_{2,n} \end{bmatrix} \quad (2)$$

where

Z_n	time shift operator e^{jT_n};
T_n	one-way transit time for the nth layer (s);
R_n	specific acoustic impedance for the nth layer (Rayl);
$F_{1,n}, F_{2,n}$	force variables for the nth layer (N);
$U_{1,n}, U_{2,n}$	velocity variables for the nth layer (m/s);
α_n	one-way loss for the layer, which may be a function of frequency (Np).

The expression involves specific acoustic impedance, R_n, one-way loss, α_n, and the one-way transit time, T_n. The layers connected to the front face represent matching layers, bond lines, metal layers, and terminate in a radiation impedance, R_W. Layers connected to the back face represent similar layers that terminate in a backing impedance, R_B. The overall electromechanical model is given in Fig. 2, with multiple two-port networks characterized by (2) connected to the front and back mechanical ports. Similarly, electrical components terminating in a transmitting source may be connected to the electrical terminals.

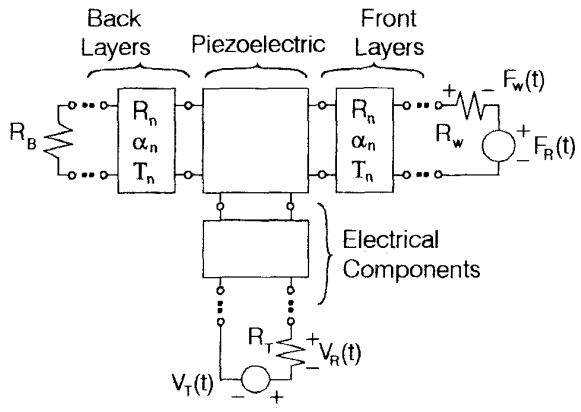

Fig. 2. Overall electromechanical model of a transducer plus electrical components terminating in a transmitting source, and mechanical layers at the front and back faces terminating in resistances. Radiation is caused by voltage V_T generating force F_W, while reception is voltage V_R caused by wave force F_R.

The one-way transmission transfer function will be considered as the radiated force over the transmitter voltage as given in

$$H_T(j\omega) = \frac{F_W(j\omega)}{V_T(j\omega)}. \tag{3}$$

Similarly, the one-way reception transfer function is the received voltage divided by the open-circuit wave force, F_R, as in

$$H_R(j\omega) = \frac{V_R(j\omega)}{F_R(j\omega)}. \tag{4}$$

Since the transducer is a linear passive reciprocal device, the two transfer functions are identical functions of frequency with the exception of a scaling constant. The transfer functions may be readily evaluated by solving the network given in Fig. 2 using well-known network analysis methods (e.g., ABCD matrices).

III. Transfer Function Design Using Computer Optimization

The transfer function of (3) is determined by the various physical parameters of the acoustic and electrical networks (e.g., layer impedance, thickness, etc.). These physical parameters can be formulated as the components of a parameter vector, $\vec{P}$. The approach is to seek $\vec{P}$ so that a desired target function, $T(j\omega)$, is achieved within some error. The error measure between $H_T(j\omega_n)$ and the target function $T(j\omega_n)$ is defined to be

$$E = \frac{1}{N}\sum_{n=0}^{N-1} \left|20\log|H_T(j\omega_n, \vec{P})| - 20\log|T(j\omega_n)|\right| \tag{5}$$

where the error, E, is the average absolute difference between the transfer and target functions evaluated in decibels, summed over N points in frequency. If the error is made sufficiently small (over a significant bandwidth), then the target function is said to have been achieved.

There are numerous methods of computer minimization of (5) subject to a target function, $T(j\omega)$, achieved by manipulating the elements of parameter vector, $\vec{P}$. A conventional steepest descent method was used here involving numerical evaluation of the gradient of E with respect to $\vec{P}$, and moving in the opposite direction of the gradient by an adjustable step factor [17]. The essential element of the design process is the selection of the target function, $T(j\omega)$. It was determined that essentially error free optimizations are achieved when the selected target function matches the underlying characteristic resonances of the transducer.

IV. Using Filter Theory to Select Suitable Target Functions

The transducer's underlying transfer function can be estimated using an approach which views the transducer as an insertion-loss filter. The reactive elements of the electrical network, the piezoelectric layer, and the acoustic layers are "inserted" as low-loss or zero-loss reactive elements between an electrical generator with a Thevenin impedance, R_T, and a radiation load with an impedance, R_W. The problem is somewhat complicated by the addition of a third port, to which the backing acoustic network, including the backing load, is connected. However, if there is low loss at this port, the filter theory concepts of energy transmission, filtering by the reactive elements, and reciprocity may be applied. The model used is equivalent to the Mason model using certain lumped-elements connected in a configuration shown in Fig. 3(a), and is equivalent to [4] (plus the addition of the loss elements noted above).

The lumped-element model of Fig. 3(a) can be used to construct a resistor-inductor-capacitor (RLC) filter model given in Fig. 3(b), using the relationships included in the figure. As a first-order model, the transducer can be viewed as a simple bandpass filter, having one series resonator and pi networks, which is valid over some bandwidth centered near the half-wave resonance of the piezoelectric layer.

The transducer configuration of interest contains matching layers making up the front network, and a backing loss with low impedance. The two matching layers are approximated by lumped LC networks using a pair of pi networks in cascade. Combining this with the previous model, a complete lumped-element insertion-loss model is constructed in Fig. 4. From filter theory, the transfer function is seen to have an all-pole form centered on the passband, since this is a ladder structure with no series resonators shunting the ladder nor any parallel resonators in series along the ladder. The series resonator of the piezoelectric layer and the pi networks, representing the matching layers, each add a resonance. In general, if there are N matching layers then there should be as many as $N + 1$ poles in the transfer function.

The number of poles in the transfer function can be studied numerically by evaluating (3) using the Mason model transfer function for a transducer with the piezoelectric series resonator and the two matching layers all set to the same (free) resonance frequency. The Mason model analysis of the transfer function is given in Fig. 5, for three widely differing loads. The plot

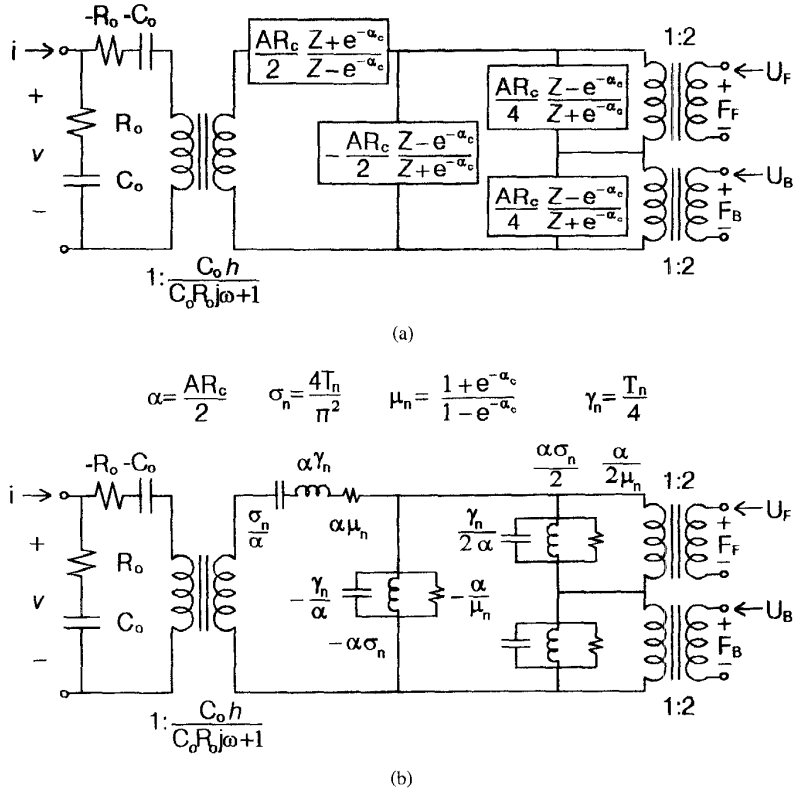

Fig. 3. Lumped-element model of the transducer: (a) the exact lumped-element model equivalent to the Mason model and (b) the narrow-band approximate model valid near the half-wave resonance of the piezoelectric layer.

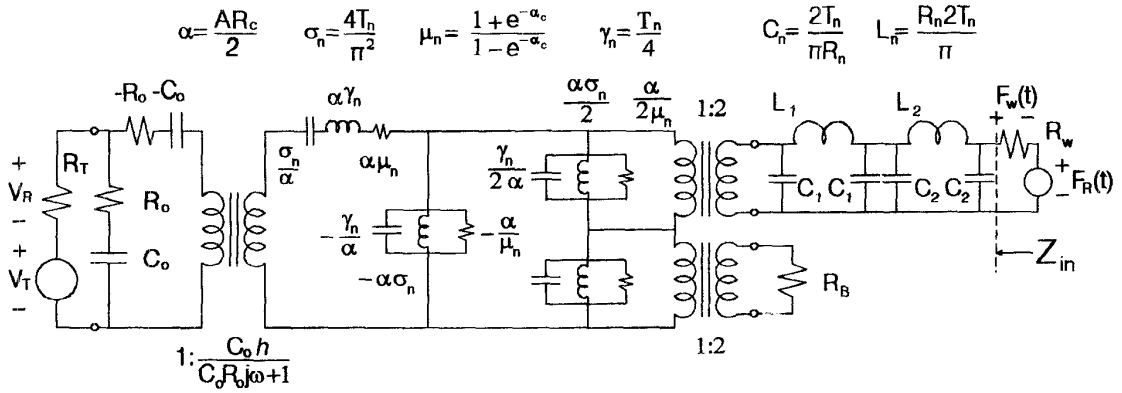

Fig. 4. Lumped-element model extended to provide a pair of pi networks representing two matching layers connecting the front port to the acoustic load.

for the 1.5 MRayl ($R_W = A$ 1.5 MRayl) load shows a bandpass transfer function with a moderate bandwidth. The three resonators become coupled so that they exhibit three widely spaced poles with a broad bandpass. For the plot with a light load of 400 Rayl ($R_W = A$ 400 Rayl) three poles are clearly seen in the transfer function. However, for the high load of 30 MRayl ($R_W = A$ 30 MRayl) there appear to be only two poles.

The pole configurations for the various acoustic loads can be explained by evaluating the reflection coefficient, ρ_2, and using a well-known relationship for insertion-loss filters [18], where the magnitude of the transfer function is determined from the terminal impedance of the acoustic port, Z_{in}, and its load, R_W as in

$$|H_T(j\omega)|^2 = 1 - |\rho_2|^2 = 1 - \left|\frac{R_W - Z_{\text{in}}}{R_W + Z_{\text{in}}}\right|^2. \quad (6)$$

The properties of Z_{in}, for the acoustic port, have been studied above by altering the load, R_W. For values of R_W approaching zero the characteristic resonances of the network are dominated by the zeros of Z_{in}. Conversely, for R_W approaching infinity, the resonances are dominated by the

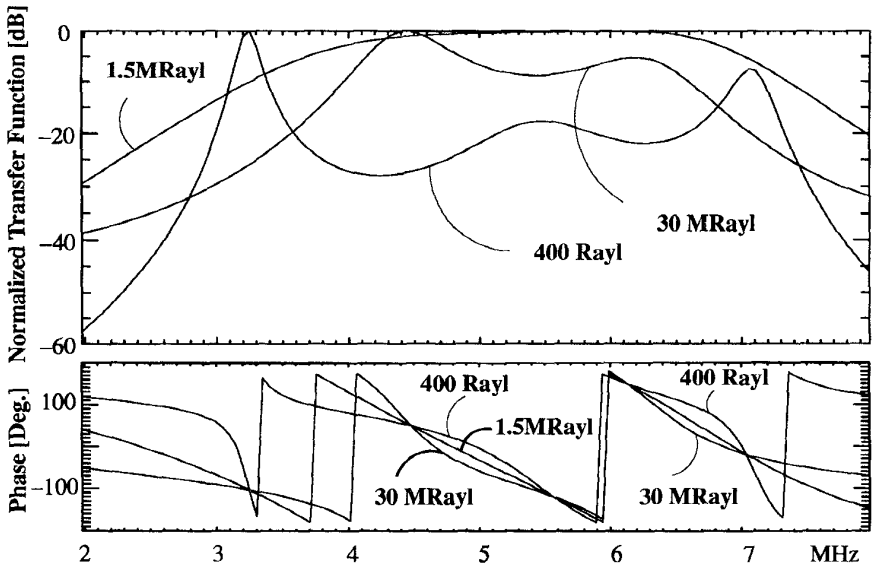

Fig. 5. Mason model transfer function evaluation for a two-matching-layer transducer with three acoustic loads consisting of tissue-like plus very light and very heavy loads. Both two- and three-pole resonances are seen.

poles of Z_{in}. For a lumped-element filter the numerator and denominator of Z_{in} may differ by only one order. The root locus of the poles making up the dynamics moves in such a manner that there are three poles seen with the light load and two poles seen with the higher load. At either extreme of the value of R_W there is light damping, and thus the high Q poles seen in the figure, while near the 1.5 MRayl loading there is greater loading and lower Q. This result supports the conclusion that we may have either N or $N+1$ poles near the band-center frequency of these filters. Consequently, the appropriate target functions used in optimization are all-pole with polynomials having N or $N+1$ poles.

V. Design Methodology for Transducers

A method for the design of the transducer transfer function and transient response can now be defined. Transducers with N matching layers are considered, which function as an N or $N+1$ pole insertion-loss filter, having low-loss reactive components. Next, the target transfer function, $T(j\omega)$, is selected to be all-pole (within the band), using a polynomial of the order N or $N+1$, which is centered on the desired frequency, as in

$$T(j\omega) = \frac{k}{X(j\{\omega - \omega_0\})}$$

where k is a scale factor, X is the desired polynomial, and ω_0 is the radian band-center frequency. Finally, the optimization algorithm adjusts the parameters of the transducer, $\vec{P}$, so as to match the poles of the given polynomial target function. The optimization uses the Mason model analysis of the transducer.

This design method is numerically demonstrated by the design of prototype transducers with bandpass transfer functions of second and third order, which require two matching layers. The basic transducer is shown schematically in Fig. 6, with a transmitter source having impedance R_T, a radiation load of impedance R_W, and an air backing of impedance R_B. Each of the elements of the design is summarized in the figure. The piezoelectric material chosen, with values given in Table I, is characteristic of PZT material (having coupling factor k_T compatible with small beam-shaped elements as in a phased array). The piezoelectric and matching layers have relatively low loss, represented by values for the various α's in the figure. The transmitter source, R_T, is arbitrarily chosen to be 50 Ω, while the radiation load, R_W, is chosen to be approximately that of tissue (1.54 MRayl). For reasons of power transfer efficiency, the layer area of the layers and piezoelectric, A, is chosen to achieve a nominal 50 Ω impedance scale for the input impedance at the electrical

TABLE I
Values for Piezoelectric Layer

Parameter	Value	Dimensions
F_p	$\frac{v^D}{2l}$	Hz
l	$\frac{v^D}{2F_p}$	Hz
R_c	32 10^6	$Rayl$
k_T	0.66	
ϵ^S	9.7 10^{-9}	F/m
A	1.43 10^{-5}	m^2
v^D	4118	m/s
α	l 1.908 $10^{-5} 2\pi f$	Np
R_0	$80/(C_0 2\pi 5\ 10^6)$	Ω

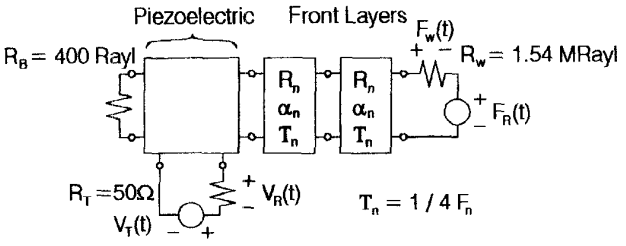

Fig. 6. Basic configuration of the series of transducers studied with one piezoelectric and two matching layers which is loaded into tissue-like media and backed by air.

terminals. The parameters for the nth matching layer are indicated in the figure with frequency, F_n, being the (free) quarter-wave resonance. The half-wave resonance, F_p, is used to characterize the piezoelectric thickness.

For convenience in displaying and interpreting the results, the transfer function $H_T(j\omega)$ is replaced by the loop response given as

$$L(j\omega) = H_T(j\omega)2H_R(j\omega). \tag{7}$$

This loop transfer is defined as the product of the transmission and reception transfer functions multiplied by a factor of two. The factor of two is associated with H_R and represents a Thevenin open circuit force of $2F_R$ for the received wave (analogous to the voltage doubling at an open-circuit transmission line), which makes the available energy of the received wave equal to the energy in the radiated wave [4]. Conceptually, the loop response in (7) represents the received signal at R_T due to excitation by the transmitter voltage V_T with a perfect radiation transfer. The loop transfer achieves a theoretical optimum of -6 dB. Transfer efficiency for one-way is easily computed using

$$\mathrm{dB}(|H_p(j\omega)|) = \frac{\mathrm{dB}(|L(j\omega)|) - 6}{2}. \tag{8}$$

For the target function, nine uniformly spaced target points were employed, which appears to have adequately covered the band between the -3 dB points of $H_T(j\omega)$. The parameter vector, $\vec{P}$, was chosen as a five-dimensional (5-D) vector involving the piezoelectric layer thickness plus the impedance and thickness of each of the two matching layers. The algorithm minimized the error value in this 5-D parameter space. The fractional bandwidth is calculated from the -3 dB (one-way transfer function) bandwidth and the band-center frequency.

Sixteen transducer designs were studied using three different polynomial shapes with differing bandwidths, as listed in Table II. The polynomial shapes were selected to permit the study of progressively wider bandwidths starting with the Bessel and progressing to Butterworth and Chebyshev in Figs. 7, 8, and 9, respectively. Table II provides full prototype details with layer thicknesses reported using the quarter-wave free resonances and acoustic impedances of the matching layers. The thickness of the PZT layer is given as the half-wave resonances, F_p. Also, Table II lists the resulting average error of the fit to the target function.

The Bessel transfer, seen in Fig. 7, covers fractional bandwidths from 45 to 70% in increments of 5%. The error of the approximation is extremely small for the cases from 50 to 65% and rises for the 70% case, suggesting that the polynomial cannot be approximated by the transducer poles at the higher design bandwidths. For the 45% case, the error of fit is good, however, the outer window impedance has been optimized to nearly that of the acoustical load. This is a second-order Bessel, which is an $N = 2$ case. It appears that fractional bandwidths above 45% are best fitted by $N + 1 = 3$ poles. For the 70% case, the shape of the transfer function appears to have higher bandwidth than the target function at the band edges, suggesting that the Q of the two outside poles is higher than that of the poles of the polynomial. The loop transfer functions, with bandwidths above 50%, achieve peak transfer functions of approximately -7.4 dB, which indicates a one-way power transfer efficiency of -0.7 dB. The two cases at 45 and 50% demonstrate a lower transfer efficiency as the dynamic transitions to the $N = 2$ case.

For bandwidths from 60 to 80%, the Butterworth transfer is given in Fig. 8. The error of fit is best for the cases covering the bandwidths from 65 to 75%, with excellent flatness in the 70% transfer function. The errors of the 60 and 65% cases show a peaking of the Q's of the outside poles and a saddle point at band-center, which suggests that the desired third-order dynamic is no longer achievable. A second-order Butterworth is evaluated at 60% bandwidth, and achieves good error fit. The 80% case develops two inflection points on either side of band-center, suggesting that the two outside poles are again becoming higher Q than the Butterworth poles and that a target function with higher ripple would fit better. All transfer functions achieve peak transfer values of approximately -7.4 to -7.9 dB for a one-way power transfer efficiency of -0.7 to -0.95 dB at these peaks.

The Chebyshev pole locations converge to that of the Butterworth as the ripple approaches zero. Consequently, it is expected that the higher bandwidths will satisfy a Chebyshev polynomial with finite ripple. The Chebyshev transfer, as seen in Fig. 9, covers bandwidths from 75 to 90% in 5% steps, and overlaps the bandwidths of the Butterworth for the 75 and 80% cases. The ripple of the target functions was adjusted at each bandwidth in order to minimize the error of the computer match. For the 75% bandwidth, with a ripple of 0.001 dB, the result is essentially a Butterworth transfer function, as can be seen in the figure. For bandwidths above 75%, excellent error matches were achieved with progressively greater ripple factors building to 1.1 dB (zero to peak ripple for the one-way Chebyshev transfer) at a bandwidth of 90%. Excellent error matches were achieved for all the cases. This suggests that the Chebyshev polynomial, with its ripple parameter, can match the inherent pole locations of the transducer over a very wide range. The transfer functions achieve peak values ranging from -8 to -8.3 dB, which correspond to power transfer efficiencies of -1 to -1.15 dB.

Inspection of Table II shows that the impedances of both matching layers increase with bandwidth for all polynomial types. This indicates that progressively greater impedance transformations of the acoustic load are required with pro-

TABLE II
FILTER PARAMETERS FOR CASES STUDIED

Case	Band	Ripple	Thickness Resonances			Impedances		Error	"Front Load"
	(%)	(dB)	(MHz).....			(*MRayl*).....		(dB)	(*MRayl*)
			PZT	Layer 1	Layer 2	Layer 1	Layer 2		
Bessel	45		5.85	5.01	4.27	3.20	1.59	.044	6.24
Bessel	50		5.86	4.96	4.58	3.80	1.74	.029	7.34
Bessel	55		5.87	4.95	4.68	4.39	1.89	.029	8.31
Bessel	60		5.88	4.95	4.77	5.00	2.04	.033	9.25
Bessel	65		5.90	4.99	4.96	5.54	2.22	.053	9.59
Bessel	70		5.91	4.97	5.02	6.17	2.40	.105	10.18
Btwrth*	60		5.90	4.88	4.73	5.05	1.79	.044	12.26
Btwrth	60		6.02	4.73	4.56	5.26	1.61	.109	16.44
Btwrth	65		5.97	4.79	4.88	6.05	1.86	.082	16.29
Btwrth	70		5.96	4.82	4.97	6.81	2.08	.029	16.51
Btwrth	75		5.95	4.84	5.04	7.63	2.32	.058	16.66
Btwrth	80		5.96	4.84	5.05	8.42	2.58	.207	16.40
Cheby	75	.001	5.96	4.81	5.02	7.72	2.30	.031	17.35
Cheby	80	0.16	6.01	4.73	4.94	9.21	2.57	.026	19.78
Cheby	85	0.75	6.06	4.67	4.91	11.0	3.03	.020	20.30
Cheby	90	2.10	6.14	4.57	4.85	13.4	3.89	.046	18.27

* 2nd order

gressively higher bandwidths. Each of the three polynomials appears to require different ratios of the inner and outer window impedances. An interesting design parameter appears to be the approximate transformed acoustic load impedance presented to the piezoelectric (assuming the matching layers were synchronously tuned), which is given by $(R_0/R_1)^2 R_W$ and recorded in Table II as the "Front Load." This transformed load impedance consistently increases with increasing bandwidth, except in the case of the third-order Butterworth where it holds a constant value of approximately 16.5 MRayl. The significance of backing loss can be judged by considering the series connection (Fig. 3) of the backing having an impedance of 400 Rayl with the much higher transformed acoustic impedances.

It is important to recall that the results in Figs. 7, 8, and 9 represent computer optimized solutions of the Mason model. The transfer functions in the figures indicate that there is always a minimal loss for the transducers, even with good matching of electrical impedance scales between transducer and source impedance. The power transfer functions for the two-matching-layer designs exhibit increasing loss with increasing bandwidth from -0.7 dB to -1.15 dB. The most important component of the loss arises from C_0, which contributes a reactive component to the electrical impedance mismatch. As can be seen in the data, the error from neglecting C_0 may be considered acceptable for many designs. It is interesting to note that if C_0 is neglected, the transfer function of the mechanical part of the transducer may be frequency scaled by simply scaling the thickness dimensions of all the mechanical components. Also, a component of the loss arises from the finite mechanical quality and dielectric quality factors of the piezoelectric, plus loss into the backing, which will be considered in a later section.

VI. THE ACHIEVABLE BANDWIDTH FOR LOW-LOSS TRANSDUCERS

The relationship of bandwidth to transmission efficiency is of considerable interest. Bode [19] and then Fano [20] provided relationships between power transfer efficiency and bandwidth when compensating networks are used to match a generator to an arbitrary fixed network. Normally, this method

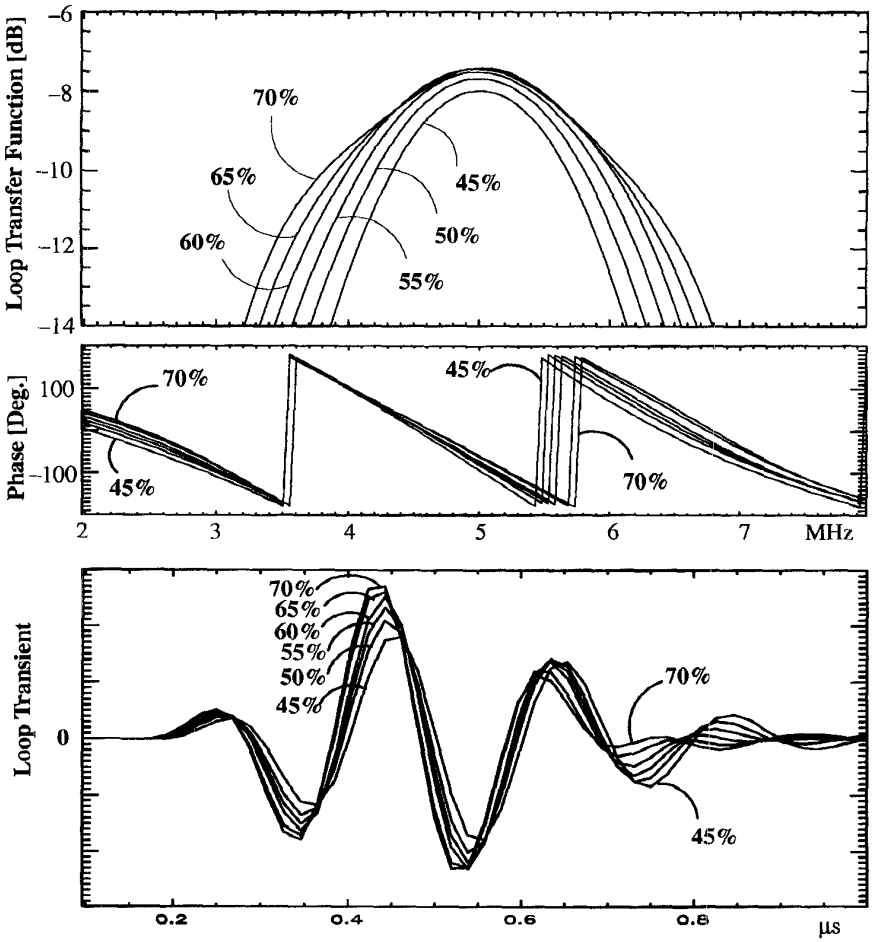

Fig. 7. Loop transfer function and transient response for transducers approximating a Bessel polynomial transfer function (squared), with fractional bandwidths from 45 to 70%. Higher bandwidths demonstrate increased edge pole Q, and lower bandwidths reduce to second-order dynamics.

is used to add a lumped-element compensating network to the electrical terminals of a transducer. However, it is possible to apply Fano's methods to the conventional matching layers. With reference to Fig. 10, Fano's compensating network is associated with the matching layers, the radiation resistance, R_W, is one load, and the piezoelectric layer and receiver resistance, R_T, make up the fixed network that is being compensated. With this we can evaluate the optimal bandwidth and transmission of the transducer.

Fano's bound applies to a purely reactive lumped-element network between the two loads, consequently, the results will only apply to low-loss transducers. The lumped-element model of Fig. 3(b) is an excellent model within the bandpass (and may be made arbitrarily exact over an extended band by adding additional reactive elements). The lumped-element model contributes three reactive components to Fig. 10: C_0 plus L_1, C_1 of the series resonator from the piezoelectric layer. In this interpretation the parallel resonators of Fig. 3(b) have been ignored on the basis that they are high in impedance compared to the matching network. Also, the electromechanical transformer of Fig. 3(b) has been absorbed into various factors of $(C_0 h)$ or its square, as well as the $2:1$ transformer into factors of two or four. Similarly, the matching network is assumed to produce transformation factors of m or m^2. Finally, all loss is set to zero, which results in a shorted backing port, $R_b = 0$, no dielectric loss, $R_0 = 0$, and all coefficients of absorption are $\alpha_n = 0$.

The basis of the performance bound lies in the Taylor series expansion of the natural log of the input reflection coefficient ρ_1, of Fig. 10. If the transfer function is a low pass that is flat within its band, f_c, then $\rho_1 = \rho_{\max}$ is also a constant over the band, f_c, and the Bode integral can be interpreted as the bandwidth times the natural log of $1/|\rho_{\max}|$. The performance bound for a single component, such as a shunting capacitor, takes the familiar form

$$\int_0^\infty \ln \frac{1}{|\rho_1(j\omega)|}\, d\omega = 2\pi f_c \ln \frac{1}{|\rho_{\max}|} \leq \frac{\pi}{2} A_1 = \frac{\pi}{R_T C_0}. \tag{9}$$

This first-order bound is most often quoted. However, the transducer of Fig. 10 requires solving for three components, making the solution much more complex. Fano showed that given the three reactive components in the network of Fig. 10,

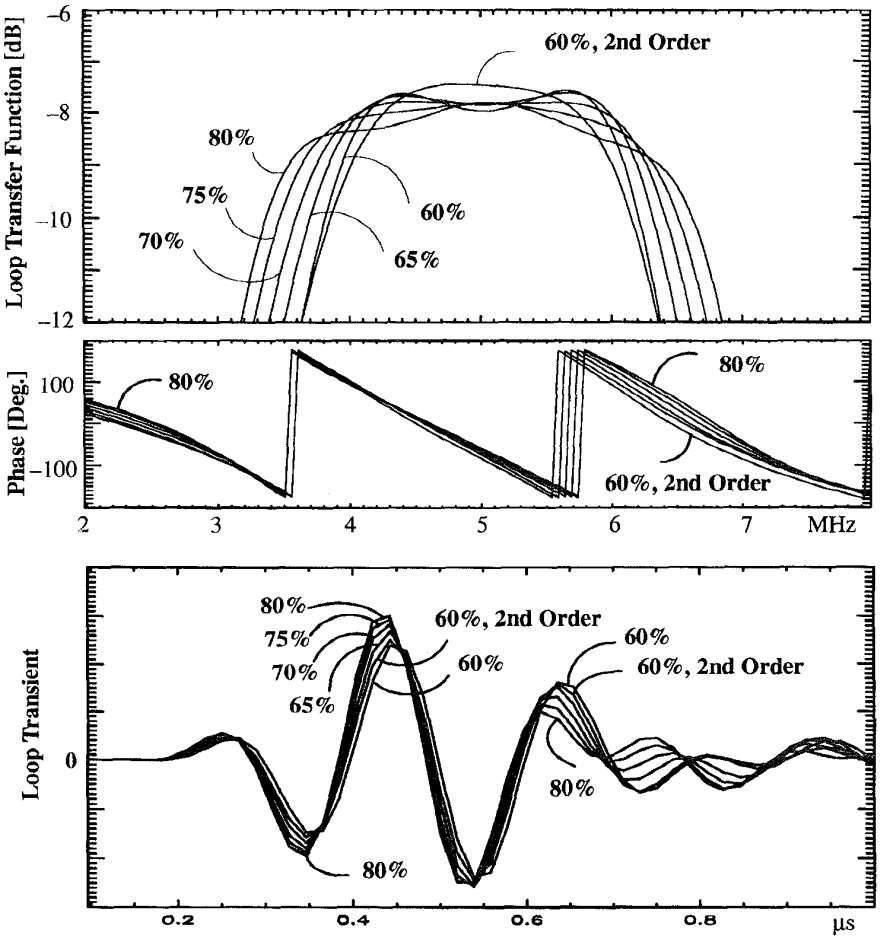

Fig. 8. Loop transfer function and transient response for transducers approximating a Butterworth polynomial transfer function (squared), with fractional bandwidths from 60 to 80%. Higher bandwidths demonstrate increased edge pole Q, and lower bandwidths reduce to second-order dynamics.

then three equations of the form

$$\int_0^\infty \omega^{\pm 2k} \ln \frac{1}{|\rho_1(j\omega)|}\, d\omega = (-1)^k \frac{\pi}{2}\left(A_{2k+1} - \frac{2}{2k+1}\sum_i \lambda_{ri}^{\pm(2k+1)}\right) \quad (10)$$

must be satisfied for $k = 0, 1, 2$ where the A_{2k+1} are the Taylor series coefficients for the natural log of the reflection coefficient and the λ_{ri} are free variables.

The coefficients, A_{2k+1}, are evaluated for the "load to be matched" by considering the subfilter formed by terminating the filter at the resistor, R_T, indicated in Fig. 10(a). Unfortunately, Fano showed that there is no general third-order solution. However, a second-order low-pass solution does exist for the network of Fig. 10(b), which can be applied to our problem by using a well-known bandshifting technique, indicated in Fig. 10(c). In the bandshifting, C_0 is resonated at the band-center frequency, ω_0, using the inductor L_0. Inductor L_1 is resonated at the same frequency by C_1, as desired. As remarked by Fano, it is well known that the bandshifting transformation produces a bandpass transfer function whose bandwidth is equal to the zero to cut off bandwidth of the low-pass filter. The Appendix solves the second-order performance bound for the low-pass filter of Fig. 10(b), which can then be directly applied to the transducer of Fig. 10(c). The resulting Fano bound is graphed in Fig. 11. The bound is plotted as a family of curves showing the reflection coefficient as a function of the normalized frequency variable

$$\frac{2\pi f}{A_1^\infty} = \frac{2\pi f}{\left(\frac{2}{C_0 R_T}\right)}. \quad (11)$$

The curves are indexed on the parameter

$$\frac{-A_3^\infty}{(A_1^\infty)^3} = \frac{1}{4}\left(\frac{C_0 R_T^2}{L_1} - \frac{1}{3}\right). \quad (12)$$

The curves give the performance bound for bandwidth versus reflection coefficient for a flat bandpass filter of the form of Fig. 10(c).

VII. Applying Fano's Bound to Low-Loss Transducers

As a test of this predicted performance bound and the ability of multilayer (nearly) quarter-wave compensation filtering,

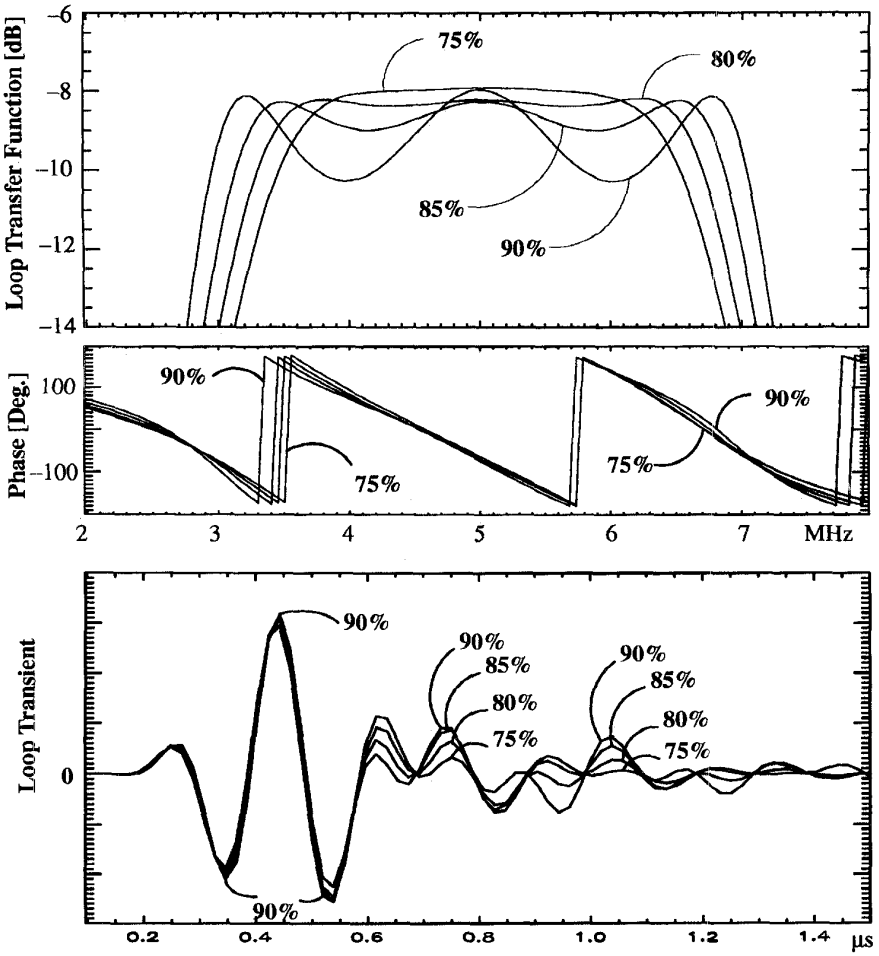

Fig. 9. Loop transfer function and transient response for transducers approximating a Chebyshev polynomial transfer function (squared), with fractional bandwidths from 75 to 90%. Progressively wider bandwidths are accommodated by higher ripple.

a transducer with a fifth-order Chebyshev transfer function centered on 5 MHz was designed, using four matching layers and a resonating inductor. This all-pole filter function is nearly the ideal flat bandpass function assumed in the analysis. The resulting bandpass, seen in Fig. 12, is approximately 5.8 MHz centered on 5 MHz for a fractional bandwidth of about 116% (−6 dB two-way, 0.6 dB ripple, 19 points, peak error of 0.6 dB). The parameters of the various (lossless) transducer components are given in Table III.

The performance bound for this transducer (and several others) is summarized in Table IV. In the table, the approximate value of $\rho_{\max}$ and the observed bandwidth (−6 dB loop) are given together with the A_1^∞ frequency scaling factor and $-A_3^\infty/(A_1^\infty)^3$ parameter that identifies the curve. Note that this test case achieves 97% of the optimal bandwidth, which can also be seen in Fig. 11 while using the appropriate frequency axis.

The performance bound of Fig. 11 can be applied approximately to the series of transducers studied earlier. Using the Mason model, the reflection coefficient, ρ_2, is given for three of the transducers in Fig. 13. These transducers have some loss (in the piezoelectric and in the air backing) such that $|\rho_1(j\omega)|$ is only approximately equal to $|\rho_2(j\omega)|$. To compare the various transducers to the bound, Table IV lists the −6 dB (two-way) bandwidths and the values of $\rho_{\max}$, which match the areas of the curves in the figure, given the bandwidths. Referring to Table IV and Fig. 11, the Butterworth 70% and Chebyshev 90% are within 80% and 79% of the optimal bandwidth, respectively. The Bessel 50% is much farther from the bound at 56% of optimal. These are good general agreements, which are probably affected by the nonideal shape of the passbands plus added loss.

The higher order Chebyshev approaches the bound most likely since its shape approaches a perfect filter. In the limit, an infinite order Chebyshev would equal the bound. In principle, the calculations in the Appendix can be repeated by inserting a specific form for $\rho_1(\omega)$ into the integrals of (13) and (14) and solving for a new set of curves as in Fig. 11. Note that the earlier transducers are constructed without the resonating inductor L_1. From this study it is concluded that transducers composed of multiple (nearly) quarter-wave layers can achieve nearly optimal low-loss performance for flat transfer functions. Moreover, it appears that this class of transducer prefers high Q pole configurations when high bandwidth is desired.

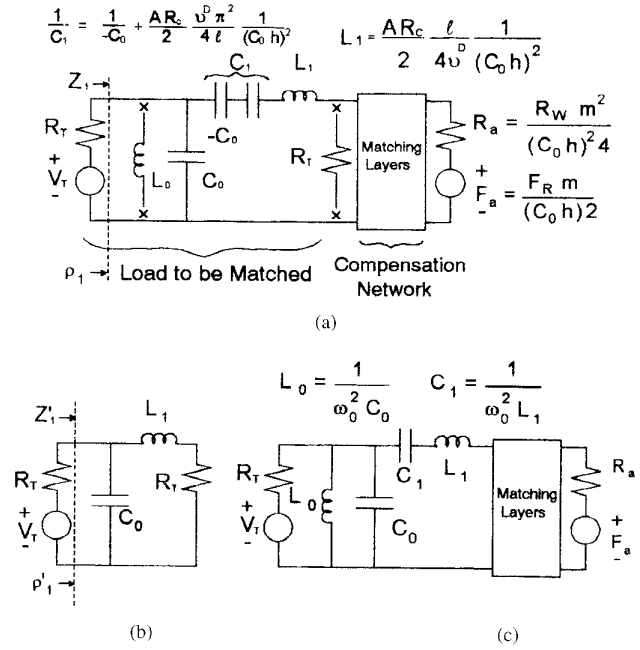

Fig. 10. The application of Fano's performance bound to multilayer compensating networks: (a) the basic electrical equivalent lumped-element network, (b) a prototype second-order low-pass filter, and (c) the bandshifted equivalent that applies to the transduces under study.

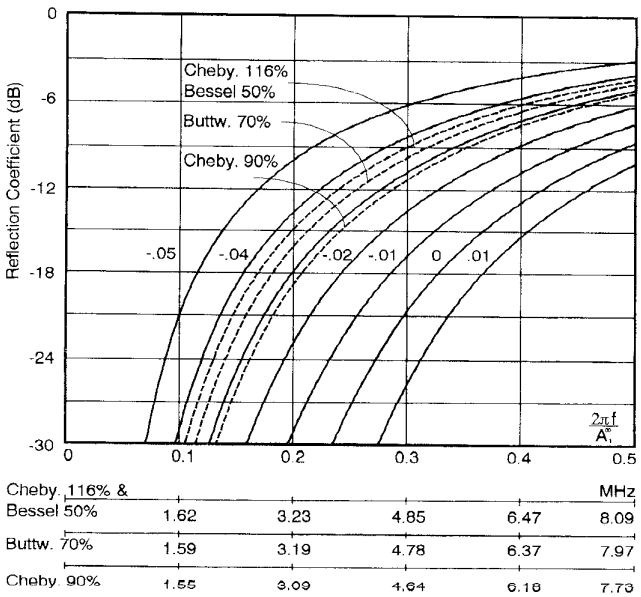

Fig. 11. Fano's second-order performance curves for reflection coefficient versus frequency, as indexed on a curve parameter. The frequency plot is versus a general frequency parameter as well as several specific frequency axes for transducers discussed in the text.

VIII. Use of Loss to Achieve Other Polynomial Configurations

The previous sections provide numerical evidence that low-loss transducers of the type studied prefer very high Q poles. Other all-pole filters require polynomials with lower Q poles. Previous work indicates that if higher loss materials are utilized, the Q's of the poles may be reduced at the expense of power transfer efficiency [16]. To evaluate this a Bessel filter (Gauss-like transfer) was synthesized using three matching layers, each having loss, plus a finite backing impedance. The target function is the reciprocal of a fourth-order Bessel polynomial band-centered on 5 MHz, and having 90% fractional bandwidth. Using 19 target points, spaced uniformly between the -6 dB (two-way) band edges, the peak error was 0.2 dB. The algorithm adjusted a parameter vector, $\vec{P}$, that included parameters for the thickness, loss,

TABLE III
Five-Pole Chebyshev 116% Components

Layer	Thickness Resonance (MHz)	Impedance ($MRayl$)
PZT	5.87	32.11
Layer 1	4.50	26.73
Layer 2	4.92	11.38
Layer 3	4.94	4.60
Layer 4	5.18	2.24

TABLE IV
Predicted Fano Bounds for Given Transducers

Transducer	$\lvert\rho_{max}\rvert$ (dB)	Bandwidth (MHz)	A_1^∞ x10^8	$-A_3^\infty/(A_1^\infty)^3$	f_c (MHz)
Cheby. 116%	-6	5.8	1.016	-0.037	5.98
Butterw. 70%	-11	3.5	1.001	-0.034	4.36
Cheby. 90%	-8.5	4.5	.9709	-0.028	5.70
Bessel 50%	-10	2.5	1.017	-0.037	4.48

TABLE V
Fourth-Order Bessel Transducer with Loss

Layer	Thickness Resonance $[MHz]$	Impedance $[MRayl]$	Loss $\alpha = *f[Hz]$
PZT	7.41	32.11	$1.66\ 10^{-4}$
Layer 1	6.35	7.89	$6.54\ 10^{-3}$
Layer 2	4.73	2.99	$6.52\ 10^{-3}$
Layer 3	4.51	1.91	$6.54\ 10^{-3}$
Backing	na	6.00	na

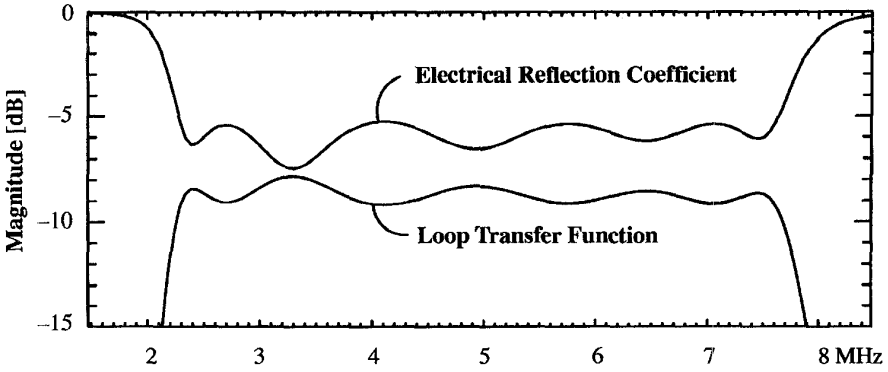

Fig. 12. The loop transfer function and reflection coefficient for a fifth-order Chebyshev 116% fractional bandwidth lossless transducer.

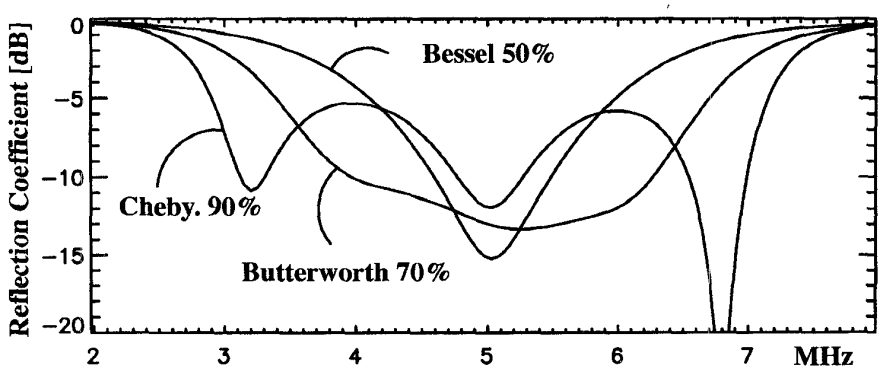

Fig. 13. The reflection coefficient, ρ_2, for three transducers from the series of low-loss designs.

and impedance of all matching layers, as well as the backing impedance. The resulting loop transfer function and transient response are shown in Fig. 13, with parameter values given in Table IV.

The transfer function is essentially a zero error fit down to -6 dB (two-way). The transient response is nearly a Gaussian envelope times a carrier, with errors less than -40 dB of the peak. Unfortunately, the transducer suffers from a transfer efficiency of -11.8 dB due to the losses that were required. However, this does prove that a great many polynomial target functions may be achieved with the basic transducer configuration.

IX. Conclusion

A modified Mason model for the transducer has been used for exact analysis and design of transducer transfer functions and/or transient responses using computer optimization. Classical filter theory applied to a lumped-element approximate model indicated that transducer transfer functions have an all-pole form (within the passband) determined by an appropriate polynomial of order N to $N + 1$, where N is the number of matching layers. A design methodology has been proposed and numerically tested using computer optimization of layer parameters to match the all-pole target polynomials. The design methodology is applicable to an arbitrary number of layers and poles.

The design methodology was tested for a series of low-loss designs using three polynomial transfer functions with progressively wider bandwidths (and higher ripple factors). It was observed that with increasing bandwidth, higher Q poles are required as a natural property of the low-loss transducers. This tendency toward higher Q with greater bandwidth requires that polynomials posses greater ripple to achieve optimization. As bandwidth is reduced, lower order polynomials are required. The significance of the backing loss can be judged by comparing it to the transformed impedance presented to the piezoelectric front face.

In general, the power transfer function is very efficient when the mismatch in impedance scales between transmitter and transducer is made small. This can be achieved by the use of transformers, area scaling, multiple piezoelectric layers, and other methods. The transducer transfer function may be frequency scaled by thickness scaling all the layers.

The application of a second-order Fano bound predicts the achievable bandwidth versus reflection coefficient performance for this class of transducers. It was found that conventional multilayer construction can achieve the optimal performance. The test case was a lossless high-order Chebyshev design exhibiting a 116% fractional bandwidth. It was demonstrated that the inclusion of loss permits the design of a broad range of pole configurations. The test case was a fourth-order Bessel transfer function, with 90% fractional bandwidth and a considerable transfer efficiency penalty.

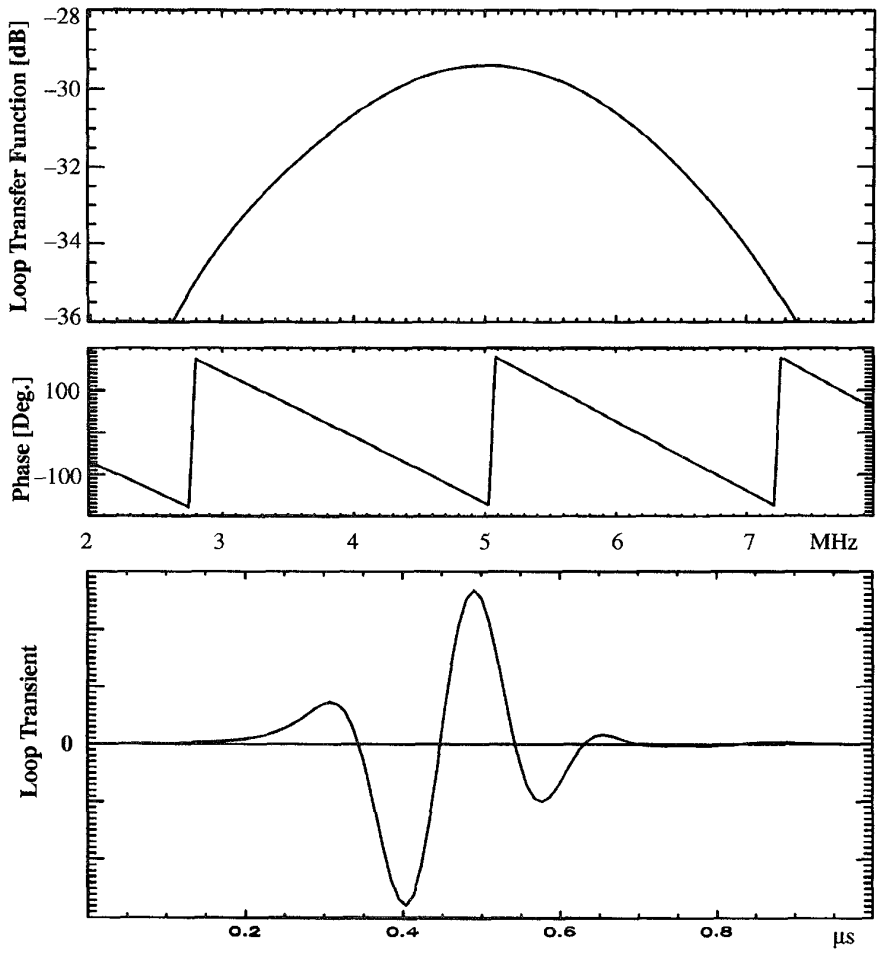

Fig. 14. The loop transfer function and transient response of a fourth-order Bessel transducer with loss.

APPENDIX

Following Fano's notation the reflection coefficient for the low-pass filter in Fig. 10(b) is

$$\rho_1' = \frac{S\left(S + \frac{1}{L_1} - \frac{1}{C_0}\right)}{S^2 + S\left(\frac{1}{L_1} + \frac{1}{C_0}\right) + \frac{2}{C_0 L_1}}.$$

The zero and poles of this rational function are

$$\lambda_{o0} = \frac{1}{C_0} - \frac{1}{L_1}$$

and

$$\lambda_{p1,2} = -\frac{1}{2C_0}\left(\frac{C_0}{L_1} + 1\right) \pm \sqrt{\left[\frac{1}{2C_0}\left(\frac{C_0}{L_1} + 1\right)\right]^2 - \frac{2}{L_1 C_0}}.$$

Evaluating the Taylor coefficients using

$$A_{2k+1}^{\infty} = \frac{1}{2k+1}\left(\sum_i \lambda_{oi}^{2k+1} - \sum_i \lambda_{pi}^{2k+1}\right).$$

The first and third coefficients are

$$A_1^{\infty} = \frac{2}{C_0 R_T}$$

and

$$A_3^{\infty} = -\left(\frac{2}{C_0 R_T}\right)^3 \frac{1}{4}\left(\frac{C_0 R_T^2}{L_1} - \frac{1}{3}\right).$$

These values can be inserted into the integral equations assuming that a flat bandpass of bandwidth, from zero to f_c, is being integrated having a reflection coefficient $\mathrm{dB}(\rho_{\max})$, expressed in decibels. The two equations to be satisfied are

$$\int_0^{\infty} \ln \frac{1}{|\rho_1(2\pi f)|}\, d2\pi f = 2\pi f_c \frac{-\mathrm{dB}(\rho_{\max})}{20\log(e)} = \frac{\pi}{2}\left(A_1^{\infty} - 2\sigma_r\right) \tag{13}$$

and

$$\int_0^{\infty} \ln \frac{(2\pi f)^2}{|\rho_1(2\pi f)|}\, d2\pi f = \frac{1}{3}(2\pi f_c)^3 \frac{-\mathrm{dB}(\rho_{\max})}{20\log(e)} = \frac{\pi}{2}\left(-A_3^{\infty} + \frac{2}{3}\sigma_r^3\right). \tag{14}$$

The solution consists of eliminating the free variable σ_r and solving for the roots of a third-order polynomial in $\mathrm{dB}(\rho_{\max})$. The solution is accomplished computationally with the results given in the graph of Fig. 11, which is similar to Fano's Fig. 7. In the figure, $\mathrm{dB}(\rho_{\max})$ is expressed as a family of curves plotted as a function of the normalized frequency variable, $2\pi f/A_1^{\infty}$, and parameterized on values of $-A_3^{\infty}/(A_1^{\infty})^3$.

REFERENCES

[1] W. P. Mason, *Electromechanical Transducers and Wave Filters.* New York: Van Nostrand, 1948.

[2] M. Redwood, "Transient performance of a piezoelectric transducer," *J. Acoust. Soc. Amer.,* vol. 33, no. 4, pp. 527–536, Apr. 1961.

[3] R. Krimholtz, D. A. Leedom, and G. L. Mathaei, "New equivalent circuits for elementary piezoelectric transducers," *Electron Lett.,* vol. 6, pp. 398–399, 1970.

[4] T. L. Rhyne, "An improved interpretation of Mason's model for piezoelectric plate transducers," *IEEE Trans. Sonics Ultrason.,* vol. SU-25, pp. 98–103, 1978.

[5] S. B. Cohn, "Optimum design of stepped transmission-line transformers," *IRE Trans. Microwave Theory Tech.,* vol. MTT-3, pp. 16–21, 1955.

[6] T. M. Reeder and D. K. Winslow, "Characteristics of microwave acoustic transducers for volume wave excitation," *IEEE Trans. Microwave Theory Tech.,* vol. MTT-17, pp. 927–941, Nov. 1969.

[7] G. Kossoff, "The effects of backing and matching on the performance of piezoelectric ceramic transducers," *IEEE Trans. Sonics Ultrason.,* vol. SU-13, pp. 20–30, 1966.

[8] C. Desilets, J. Fraser, and G. S. Kino, "Transducer arrays suitable for acoustic imaging," in *IEEE Proc. 1975 Ultrasonics Symp.,* pp. 148–152.

[9] T. Inoue, M. Ohta, and S. Takahashi, "Design of ultrasonic transducers with multiple acoustic matching layers for medical application," *IEEE Trans. Ultrason., Ferrelect., Freq. Contr.,* vol. UFFC-14, pp. 8–15, 1987.

[10] J. H. Goll and B. A. Auld, "Multilayer impedance matching schemes for broadbanding of water loaded piezoelectric transducers and high Q electric resonators," *IEEE Trans. Sonics Ultrason.,* vol. SU-22, pp. 52–53, 1975.

[11] J. H. Goll, "The design of broad-band fluid-loaded ultrasonic transducers," *IEEE Trans. Sonics Ultrason.,* vol. SU-26, pp. 385–393, 1979.

[12] A. R. Selfridge, R. Baer, B. T. Khuri-Yakub, and G. S. Kino, "Computer optimized design of quarter-wave acoustic matching and electrical matching networks for acoustic transducers," in *Proc. IEEE Ultrasonics Symp.,* 1981, pp. 644–648.

[13] G. R. Lockwood and F. S. Foster, "Modeling and optimization of high-frequency ultrasound transducers," *IEEE Trans. Ultrason., Ferroelect., Freq. Contr.,* vol. 41, pp. 225–230, 1994.

[14] M. Van Crombruge and W. Thompson, Jr., "Optimization of the transmitting characteristics of a Tonpilz-type transducer by proper choice of impedance matching layers," *J. Acoust. Soc. Amer.,* vol. 77, pp. 747–752, 1985.

[15] G. S. Kino, *Acoustic Waves: Devices, Imaging, and Analog Signal Processing.* Englewood Cliffs, NJ: Prentice-Hall, 1987.

[16] T. L. Rhyne and S. Panda, "Design implications of using transducer noise figure as the basis of sensitivity," in *Proc. IEEE Ultrasonics Symp.,* 1993, pp. 1167–1170.

[17] W. H. Press, S. A. Teukolsky, W. T. Vetterling, and B. P. Flannery, *Numerical Recipes in C.* New York: Cambridge Univ. Press, 1992.

[18] R. Saal and E. Ultrich, "On the design of filters by synthesis," *IRE Trans. Circuit Theory,* vol. CT-6, pp. 284–317, 1958.

[19] H. W. Bode, *Network Analysis and Feedback Amplifier Design.* Princeton, NJ: Van Nostrand, 1945.

[20] R. M. Fano, "Theoretical limitations on the broadband matching of arbitrary impedances," *J. Franklin Inst.,* pp. 57–83, 139–154, 1950.

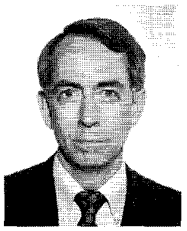

Theodore L. Rhyne (M'67) was born in Summit, NJ, on August 31, 1944. He received the S.B. degree in 1966, the S.M. and E.E. degrees in 1972, and the Sc.D. degree in 1976, all in electrical engineering from the Massachusetts Institute of Technology, Cambridge.

From 1966 to 1968 he worked in Omega radio navigation at the Northrop Corporation. From 1968 to 1970, while in the Army Signal Corps, he managed the development of Loran C navigation equipment. From 1970 to 1976 his graduate work developed optimal filtering of Loran C signals for his master's thesis and ultrasonic instrumentation plus tissue characterization for his doctoral thesis. His graduate work was followed up by a year of postdoctoral research at the Massachusetts General Hospital from 1976 to 1977. He worked on sonar applications at Bolt Beranek and Newman from 1977 to 1984, and participated in the analysis of gunshot sounds for the House Select Committee on Assassination. From 1984 to 1990 he was Director of Research and Development for Marquette Electronics. He is currently developing ultrasonic imagers as a staff member of the Applied Science Laboratory of GE Medical Systems.

Dr. Rhyne is a member of the Acoustical Society of America, the America Institute of Ultrasound in Medicine, and Sigma Xi.